Tribology Letters manuscript No.
(will be inserted by the editor)

Gauging Persson theory on adhesion

Anle Wang · Martin H. Müser

Received: date / Accepted: date

Abstract In this work, we propose three amendments to Persson's contact mechanics theory, the most important one being a modification of the way in which the stress distribution broadens with increasing resolution of random-roughness features. The three adjustable coefficients of our treatment are gauged on existing reference data and tested against results of the contact-mechanics challenge and a new set of data for adhesive slabs of finite width. Although the coefficients turn out to be of order unity, their problem-specific tuning is required to achieve highly accurate results, such as an essentially perfect dependence of contact area on load for non-adhesive, self-affine solids. Despite an overall convincing agreement between theory and full simulations, we find it to be intrinsically impossible to make the theory reflect the exact asymptotics of the stress distribution at small and large stresses. In addition, we find that the transition from small to large contact happens too abruptly with decreasing thickness of the elastic slab.

1 Introduction

Persson's approach to contact mechanics of nominally flat surfaces has proven to be a theory with predictive power [1,2]. As described in more detail in the theory section of this paper, it is based on the ideas of renomarlization group theory. As such, it is not an exact theory. However, it is sufficiently accurate to correctly predict or reproduce the functional form of quite a few dependences. The relation between real contact area and load across all tested regimes and geometries: (i) the linear relation between relative contact area a_r (defined as the ratio of true and apparent contact area) and the nominal pressure p at small p [3–11], (ii) the $a_\mathrm{r} \propto p^{1/(1+H)}$ relation at pressures that are so small that only one meso-scale asperity remains in contact [12,13], where H is the Hurst roughness exponent, (iii) the approach of full contact at large p in a nominally flat contact [14, 11,15] or that to the continuum solution in a Hertzian contact geometry [15,16].

Furthermore, Persson theory (iv) correctly identifies the logarithmic dependence of the mean interfacial separation (or, in brief, the mean gap, $\bar{u}$) on load for intermediate p [17–19] and the crossover to different scaling at large loads [20]. It correctly reproduces (v) the way in which $\bar{u}$ depends on the ratio of $\lambda_\mathrm{s}/\lambda_\mathrm{r}$ at a given reduced pressure p^* [11] — λ_s and λ_r being the short wavelength cutoff and the roll-off wavelength, respectively while $p^* \equiv p/E^*\bar{g}$, where E^* is the contact modulus and $\bar{g}$ is the rms-gradient of the surface height. Also numerically accurate (vi) stress distribution function [7] and (vii) gap distribution function [17, 19] have appeared to be reproduced almost exactly, although, we are going to somewhat challenge claim (vi) in this paper. Moreover, (vii) spatial correlations of the stress in contacts are correctly identified to decay as $1/\Delta r^{1+H}$ [21,22], while bearing models, which ignore long-range elastic deformation, are confined to follow a $1/\Delta r^{2(1+H)}$ scaling, irrespective of their specific details [22]. The list could be continued with comments on how readily (viii) finite thickness of slabs [23], (ix) adhesion [24,25], (x) anisotropic roughness [26], or (xi)

A. Wang
INM – Leibniz Institute for New Materials, Campus D2 2, 66123 Saarbrücken, Germany

A. Wang · M. H. Müser
Department of Materials Science and Engineering, Saarland University, Campus C6 3, 66123 Saarbrücken, Germany E-mail: martin.mueser@mx.uni-saarland.de

plasticity is included [27], although rigorous, numerical tests of the last claim have not yet been disseminated.

Despite all its advantages, the theory may still have some room for improvement. One potential problem is that the calculation of the elastic energy and the broadening of the interfacial stress distribution $\Pr(\sigma)$ has so far been handled in a slightly inconsistent fashion. Furthermore, the modifications to the elastic energy calculations were gauged empirically on data that is certainly less reliable than that from accurate, brute-force simulations, for which surface topographies, elastic properties, etc., are known, in principle, to arbitrary precision. In addition, numerically rigorous tests of the predicted $\Pr(\sigma)$ have so far been impeded by the extremely slow convergence of $\Pr(\sigma)$ [24], or were restricted to small dimensions [28] or to adhesion that is long-ranged at the smallest scale [25].

In this work, we set the corrections to the elastic energy on a common footing with corrections to the way in which $\Pr(\sigma)$ broadens as roughness features are resolved at smaller and smaller scales. In addition, we parameterize the corrections on the most accurate, available data for adhesionless contacts and some data of the Tribology Letters contact-mechanics challenge disseminated in this issue of Tribology Letters [29]. We also fine-tune a prefactor used to estimate the propagation of cracks in the treatment of adhesive contacts. Finally, we test the quality of our parameterization of Persson theory against data from the contact-mechanics challenge and against new, numerical data for adhesive systems. We have abstained from including the – as we believe – improved parameterization of Persson theory into the contact mechanics challenge, as our data would have had to be labeled as "post-dictions" rather than as predictions, whereby they would have violated the conditions for entering the competition, in addition to having been produced nine months after the submission deadline for entering the competition.

The remainder of this paper is organized as follows: In section 2, Persson theory and our amendments to it are presented as well as our numerical approach. Section 3 contains a comparison of the theoretical predictions to brute-force simulations. Conclusions are drawn in section 4.

2 Theory and Methods

2.1 Comment on notation and variables

Throughout this work, the same notation is used as that in the contact-mechanics challenge [29]. This includes the assumption of the small-slope approximation.

In addition, reduced units are indicated with a star. For example, p^* is the dimensionless pressure defined as $p^* \equiv p/E^*\bar{g}$, where $\bar{g}$ is the root-mean-square gradient of the surface, while $\sigma^* \equiv \sigma/E^*\bar{g}$. Anybody interested in real numbers can multiply quantities of dimension pressure with their own preferred numbers, e.g., with 25 MPa when being interested in soft-matter systems.

We also note that we make a minor shift in terminology in respect to Persson theory, which, however, leaves equations unaffected. Persson uses the concept of magnification, i.e., when stating that a problem is considered at a magnification of ζ, he assumes that only those random roughness features are resolved that have a wavelength equal or greater than $\mathcal{L}/\zeta$. We use the concept of resolution: when the resolution is said to be q, we imply that only those random roughness features with wave vectors $|\mathbf{q}'| \leq q$ are considered.

2.2 Persson theory for adhesive contacts

Persson theory is a renormalization-group approach to contact mechanics. It starts from the solution of a contact mechanics problem at a coarse scale that ignores all random roughness features of wave vectors larger than a given wave number q_0. The simplest case is that of a nominally flat surface of linear dimension $\mathcal{L} = 2\pi/q_0$, which is treated as if it were repeated periodically in the plane. In that case, the interfacial distribution is a simple delta-function

$$\Pr(\sigma, q_0) = \delta(\sigma - p_0), \tag{1}$$

where p_0 is the nominal contact pressure. If a flat-punch, a Hertzian, or, any other deterministic contact geometry were the starting point, the initial stress distribution function would have to be modified accordingly, i.e., $\Pr(\sigma, q_0)$ and p_0 would need to be spatially resolved.

When small-scale roughness at an (arbitrary) wave vector $\mathbf{q}$ is added, the stress distribution broadens due to the additional undulations within the contact zone. For a system that is isotropic and homogeneous in the plane, the standard deviation of the stress (assuming full contact, see also appendix A) is given by

$$\Delta p(\mathbf{q}) = \frac{qE^* f(q)}{2}\,|\tilde{h}(\mathbf{q})|, \tag{2}$$

where E^* is the contact modulus, q the magnitude of $\mathbf{q}$, and $\tilde{h}(\mathbf{q})$ the Fourier transform of the real-space height profile $h(\mathbf{r})$ given by

$$\tilde{h}(\mathbf{q}) = \frac{1}{A}\int_A d^2r\, e^{-i\mathbf{q}\cdot\mathbf{r}} h(\mathbf{r}). \tag{3}$$

The factor $f(q)$ in equation (2) depends on the system under consideration. For a slab of finite width with a constant-stress boundary condition on the surface opposite to the interface, it reads [23]

$$f(q) = \frac{\cosh(2tq) - 2(qt)^2 - 1}{\sinh(2qt) + 2qt}, \tag{4}$$

where t is the thickness of the slab. For a semi-infinite solid, $t \to \infty$, $f(q) = 1$, while for a thin beam, $t \to 0$, $f(q) = (qt)^3/6$.

The broadening of the pressure distribution is realized with a kernel function $K(\sigma, \sigma', \Delta p)$ (details on it further below and in appendix B) according to

$$\mathrm{Pr}(\sigma, q^+) = \int_{\sigma_\mathrm{a}^+}^{\sigma_\mathrm{p}} d\sigma' K(\sigma, \sigma', \Delta p) \mathrm{Pr}(\sigma', q^-). \tag{5}$$

Here, $\mathrm{Pr}(\sigma, q)$ reflects the interfacial stress distribution when all (random) undulations with wave vector $q' < q$ are resolved. q^- is the wave number just below q, while q^+ is marginally larger. The upper limit of the integral on the right-hand side of equation (5), σ_p, is the potentially scale-dependent indentation hardness [27], while σ_a denotes the maximum adhesive stress at the given resolution q [30], i.e., any local interfacial stress at the new resolution q may not exceed the given hardness while local tensile stresses must be less than that needed for the propagation of a center crack. Since we ignore plasticity in the present work, we replace σ_p with infinity in the following.

At a given resolution q, an integral over $\mathrm{Pr}(\sigma)$ yields the scale-dependent relative contact area

$$a_\mathrm{r}(q) = \int_{-\sigma_\mathrm{a}^+}^{\infty} d\sigma \, \mathrm{Pr}(\sigma, q). \tag{6}$$

An important assumption in the theory now is that the way in which the stress distribution broadens at a given contact point is not very sensitive to the stress at a given location. This is certainly meaningful for contact points far way from a contact line, but potentially problematic otherwise [31,32]. However, making this approximation, the kernel function only needs to represent the first two moments of the stress broadening, which is why it can be approximated as a Gaussian. However, when broadening encompasses the simultaneous resolution of several $\mathbf{q}$ vectors, care needs to be taken to satisfy the boundary condition, e.g., points that reach a stress of σ_a are taken to be no longer part of the contact. To reflect this boundary condition, a mirror Gaussian is added so that the kernel function

$$K(\sigma, \sigma', \Delta p) = \frac{e^{-(\sigma-\sigma')^2/2\Delta p^2} - e^{-(\sigma+\sigma'-2\sigma_\mathrm{a})^2/2\Delta p^2}}{\sqrt{2\pi\Delta p^2}} \tag{7}$$

keeps the first moment of the stress distribution unchanged while satisfying the boundary condition. The mathematical justification for the mirror Gaussian can be derived by mapping the integral formulation of Persson theory onto a diffusion equation with an absorbing boundary condition at the smallest allowed stress [1,2].

Persson relates the adhesive pull-off stress to the scale-dependent surface energy $\gamma(q)$ through the Griffith criterion

$$\sigma_\mathrm{a}(q) = \sqrt{qE^* f(q)\gamma(q)}, \tag{8}$$

thereby deferring the calculation of $\sigma_\mathrm{a}(q)$ to that of $\gamma(q)$.

Ignoring that roughness can increase the true contact area, one can gain surface energy where surfaces touch microscopically, but the elastic energy needed to comply to the counter face has to be subtracted at each resolution. Therefore, $\gamma(q)$ satisfies the equation

$$a_\mathrm{s}(q)\gamma(q) = a_\mathrm{s}(q_\mathrm{s})\gamma_\mathrm{s} - \sum_{|\mathbf{q}'|>q} a(q') u_\mathrm{ela}^{(\mathrm{f})}(\mathbf{q}) \tag{9}$$

where γ_s is the surface energy at the smallest scale and $u_\mathrm{ela}(\mathbf{q})$ the elastic energy of mode $\mathbf{q}$ in full contact

$$u_\mathrm{ela}^{(\mathrm{f})}(\mathbf{q}) = \frac{qE^* f(q')}{4} |\tilde{h}(\mathbf{q}')|^2. \tag{10}$$

A negative value of $\gamma(q)$ in equation (9) is set to zero.

To conclude the summary of Persson theory used in this work, we state that the work done on the system, $\int d\bar{u} p_0(\bar{u})$ must be equal to the change of the net potential energy per unit area, i.e.,

$$U = -a(q_\mathrm{s})\gamma_s + \sum_{\mathbf{q}} a(q) u_\mathrm{ela}^{(\mathrm{f})}(\mathbf{q}). \tag{11}$$

Since one cannot preset $\bar{u}$ in Persson theory but only p_0, the relation $dU = p_0 d\bar{u}$ is transformed into $d\bar{u} = dp(dU/dp)/p$ so that the pressure-dependent mean gap can be calculated via

$$\bar{u}(p_0) = -\int_{p_0}^{\infty} dp \frac{U'(p)}{p}, \tag{12}$$

given that $\bar{u}(p \to \infty) = 0$.

2.3 Amendments to Persson theory

Two important approximations in Persson theory are that (a) higher modes in displacement and thus stress are excited when non-contact is created and that (b) non-contact is nucleated with a larger probability in the valleys than in the flanks or on the peaks. These two effects cause opposite corrections to the broadening of the stress distribution: (a) leads to an increased

and (b) to a decreased stress broadening, whereby the contact area increases with respect to the original formulation of the theory. Without being in a position to rationalize why a previous study [32] found effect (b) to dominate (a), we analyze next, how effect (b) should be incorporated into a modification of the theory.

Assume that the true Fourier coefficient of the displacement field $\tilde{u}_{\rm t}(\mathbf{q})$ is a little less in magnitude than that considered in Persson theory, $\tilde{u}_{\rm P}(\mathbf{q})$, i.e.,

$$|\tilde{u}_{\rm t}(\mathbf{q})| = (1-\varepsilon)|\tilde{u}_{\rm P}(\mathbf{q})|. \tag{13}$$

Both, the kinetic energy and the pressure variance Δp^2 associated with the broadening due to mode $\mathbf{q}$ are then only $(1-\epsilon)^2$ times the originally anticipated value. Therefore, if the potential energy of mode $\mathbf{q}$ is corrected with a weighting factor $W\{a_{\rm r}(q)\}$ according to

$$u_{\rm ela}(\mathbf{q}) = a_{\rm r}(\mathbf{q})\frac{qE^* f(q')W\{a_{\rm r}(q)\}}{4}|\tilde{h}(\mathbf{q})|^2, \tag{14}$$

then the standard deviation of the stress needs to be modified with the same factor from equation (2). Thus,

$$\Delta p(\mathbf{q}) = \sqrt{W\{a_{\rm r}(q)\}}\frac{qE^* f(q)}{2}|\tilde{h}(\mathbf{q})|. \tag{15}$$

Persson has so far applied the correction factor $W(a_{\rm r})$ only to the elastic energy but not to the stress broadening. He finds the relation

$$W_{\rm P}(a_{\rm r}) = 1 - c_1(1-a_{\rm r}^2) \tag{16}$$

with $c_1 = 0.55$ to be useful [24]. We augment it with an additional term and use

$$W(a_{\rm r}) = 1 - c_1(1-a_{\rm r}^2) - c_2(1-a_{\rm r}^4) \tag{17}$$

instead. Our coefficients $c_1 = -2/9$ and $c_2 = 2/3$ are gauged on an analytical formula [32] for the relative contact area, which provides an excellent description of numerically rigorous results [11], in which finite-size, self-affine, and continuum corrections were included, see Figure 1. The correction factor $W(a_{\rm r})$ remains larger than one half for any value of $0 \le a_{\rm r} \le 1$, which means that it is of order unity. It could be further adjusted to reproduce the target $a_{\rm r}(p^*)$ relation even more closely. However, we do not see that this would benefit the description of any property other than $a_{\rm r}(p^*)$. Likewise, we do not consider an independent treatment of the weight functions for stress broadening and elastic energy for small adhesion, which one could motivate from the existence of large-q modes.

A quasi-exact reproduction of numerical reference data on the $a_{\rm r}(p^*)$ relationship — at least for H taking the values $H = 0.3$, 0.5, and 0.8 — is

$$a_{\rm r}(p^*) = {\rm erf}(1.9p^*)\{1 - a_0^2(p^*)\} + a_0^3(p^*) \tag{18}$$

with

$$a_0(p^*) = {\rm erf}(1.45p^*). \tag{19}$$

This last function, $a_0(p^*)$, reflects the asymptotic behavior for adhesionless, semi-infinite solids at large p^*. It is almost identical to that in the original Persson theory [1], $a_0(p^*) = {\rm erf}(\sqrt{2}p^*)$, based on $W(a_{\rm r}) \equiv 1$. Equation (18) is used for our fine tuning of the coefficients c_1 and c_2.

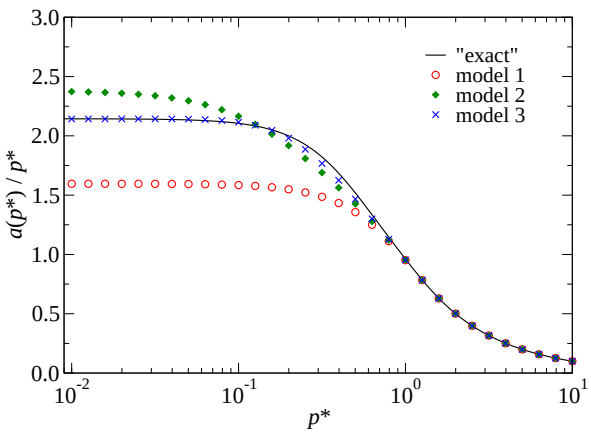

Fig. 1 Ratio of relative contact area and reduced pressure, $a_{\rm r}(p^*)/p^*$ as a function of reduced pressure. The solid line represents quasi-exact numerical data on self-affine surfaces with different Hurst roughness exponents, see Equation(18). Model 1 uses no corrections to the stress broadening, i.e., $c_1 = c_2 = 0$ in equation (17). Model 2 takes parameters that were obtained by Persson for the fine-tuning of the elastic energy $c_1 = 0.55$, $c_2 = 0$, while the parameters in model 3, $c_1 = -2/9$, $c_2 = 2/3$, were adjusted to closely match $a_{\rm r}(p^*)/p^*$ from Equation(18).

Note that neither the weight-function $W(a_{\rm r})$ nor the thickness or potential gradient corrections expressed in $f(q)$ alter the functional form of the stress distribution in the *adhesionless* case. Irrespective of their parameterization, the broadening of the stress distribution is determined by an effective mean-square surface-height gradient

$$\bar{g}_{\rm eff}^2 \equiv \sum_{\mathbf{q}} W\{a_{\rm r}(\mathbf{q})\}f(q)|\tilde{h}(\mathbf{q})|^2 \tag{20}$$

so that

$$\Delta p = E^*\bar{g}_{\rm eff}, \tag{21}$$

replaces the "usual" $\Delta p = E^*\bar{g}$ relation. The stress distribution at the small wavelength cutoff (adhesionless but potentially finite width) remains to satisfy

$$\Pr(\sigma) = K(\sigma, p_0, \Delta p). \tag{22}$$

The contact-area load relationship can now be written as in equation (18), when replacing p^* with $p^*\bar{g}/\bar{g}_{\mathrm{eff}}$.

Finally, we also take the liberty to slightly modify the Griffith criterion. First, we allow for a constant prefactor on the r.h.s. of equation (8) different than one, that is, we take σ_{a} to be twice the given value. The reasons for this correction could be that the detached shapes usually differ from circles. Also the presence of curvature from modes other than the one associated with wavevector $\mathbf{q}$ might matter. Second, whenever σ_{a} exceeds the local theoretical adhesive stress (that is, the ratio of surface energy and decay length, γ/ρ), we only allow for a maximum tensile stress of γ/ρ.

2.4 Numerical methods

We use the Green's function molecular dynamics (GFMD) method [33] to model linearly elastic contacts between solids with self-affine surface roughness. The method has been described numerous times in the literature.

Comparisons of our theoretical data are made to a large degree of published data, including that disseminated in the contact-mechanics challenge in this issue of Tribology Letters. However, we augment this data with additional simulations on adhesive, elastic slabs with finite thickness t. The specification of our system is similar to that used in the contact-mechanics challenge. However, the new system is smaller and adhesion a little less short ranged than that of the challenge so that our additional simulations do not necessitate an excessive amount of computational resources. Specifically, the ratio of system size and roll-off wavelength was reduced to $\mathcal{L}/\lambda_{\mathrm{r}} = 2$, the ratio of roll-off to short wavelength cutoff to $\lambda_{\mathrm{r}}/\lambda_{\mathrm{s}} = 128$, and the Tabor parameter to $\mu_{\mathrm{t}} = 1$. The root-mean-square gradient of the height topography remained at $\bar{g} = 1$.

Although our current treatment is just at the boarder between short- and long-range adhesion at the finest scale, we compare our simulation data to a theory assuming short-range adhesion. This is still meaningful, as adhesion effectively becomes quickly short ranged when the length scale of observation exceeds λ_{s}.

3 Results

3.1 Comparison to contact-mechanics challenge data

In this section, we compare our three variants of Persson theory to the data of the contact-mechanics challenge. Since our amendments to Persson theory were fitted to reference data on $a_{\mathrm{r}}(p^*)$, it is natural to first investigate the extent with which this procedure benefits the prediction of the stress distribution. Figure 2 compares the performance of the three discussed parameterizations (or models) to the (adhesionless) GFMD reference data from the contact-mechanics challenge. For the largest part of the diagram, the data is original data of the $2^{16} \times 2^{16}$ simulation. However, for reduced stresses $\sigma^* \equiv \sigma/E^*\bar{g}$ less than 0.04, we performed continuum corrections as described in references [7,11] by incorporating information from smaller simulations. The most refined approach, model 3, does not only produce the most accurate relative contact area — $a_{\mathrm{r}} = 0.0214$ versus $a_{\mathrm{r}}(\mathrm{GFMD}) = 0.0202$ — but it appears to match the whole stress distribution better than both model 1 ($a_{\mathrm{r}} = 0.0237$) and model 2 ($a_{\mathrm{r}} = 0.0159$).

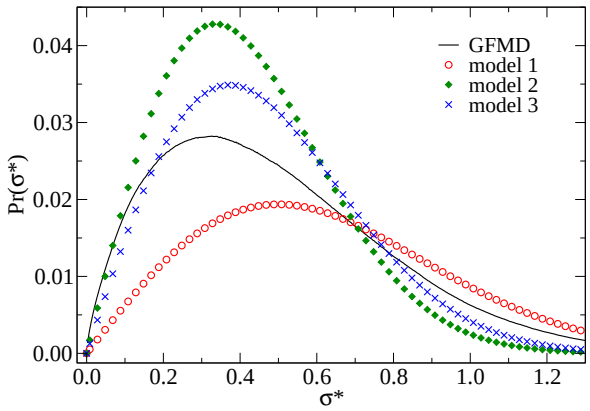

Fig. 2 Stress-distribution function $\mathrm{Pr}(\sigma^*)$ for the non-adhesive case. The models are defined in the caption of figure 1.

A refined analysis of the numerical distribution function $\mathrm{Pr}(\sigma^*)$, presented in Figure 3, reveals two features that are not possible to incorporate at the present level of the theory, no matter how the weight function $W(a_{\mathrm{r}})$ is designed: First, the asymptotic behavior of $\mathrm{Pr}(\sigma^*)$ at small stresses is clearly sub linear. This observation is confirmed with similar exponents in preliminary simulations employing $H = 0.3$ and $H = 0.5$ in addition to $H = 0.8$. The theory predicts linearity by design, no matter how the weight function $W(a_{\mathrm{r}})$ is defined, i.e., at the current level of the theory, $\mathrm{Pr}(\sigma^*)$ for linearly elastic, adhesionless contacts is restricted to take the shape of the kernel function in equation (7) $\sigma' = p_0$ and $\Delta p = E^*\bar{g}/2$. The second issue is that the asymptotic behavior at large σ^* is proportional to $\exp(-2\sigma^{*2})$, which is similar to that of the original Persson theory with $W(a_{\mathrm{r}}) \equiv 1$, albeit with a smaller prefactor, see also Figure 2. Again, no modification of the weight function $W(a_{\mathrm{r}})$ will succeed in exactly reproducing the prefac-

tor and the argument in the exponent of the asymptotic Gaussian at the same time.

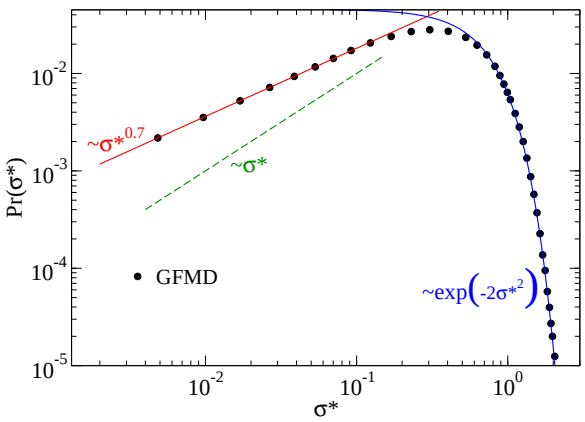

Fig. 3 Same GFMD data as in figure (2), however, in a double logarithmic representation. The asymptotic behavior for large and small stresses is included.

The crux thus is that the given double Gaussian kernel does not allow one to reproduce simultaneously the mean and the variance of the contact stress. The refined model 3 predicts the best mean, while the original model 1 estimates the second moment the most accurately. However, model 3 twice outperforms model 2. These claims are quantified in table 1. We note that properties besides the second moment of the stress distributions may also somewhat deteriorate when applying the weight functions not only to the elastic stress calculations but also to the contact-area calculations. This concerns in particular the dependence of the mean gap on load.

	GFMD	model 1	model 2	model 3
$\bar{\sigma}_c$	0.4963	0.6264	0.4215	0.4670
$\langle\delta\sigma_c^2\rangle$	0.0908	0.1071	0.0484	0.0595

Table 1 First and second moment of the contact stress as obtained in the adhesionless version of the set-up in the contact-mechanics challenge [29] at an external pressure of $p^* = 0.01$. The models are defined in the caption of figure 1.

So far, only adhesionless contacts have been considered. We now include adhesion and analyze in Figure 4 to what extent the various variants of the theory reflect the adhesion-mediated changes in the stress distribution function. The trend is identical to the previous one: The most refined variant, namely model 3, reproduces $\Pr(\sigma^*)$ best, in particular near the maximum of the distribution function. However, the original model gives the best asymptotic behavior at large σ^*.

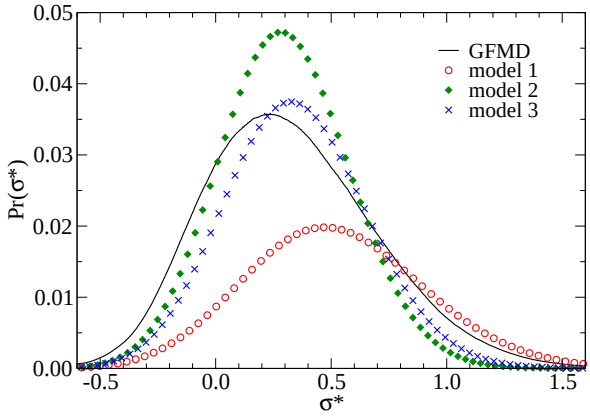

Fig. 4 Interfacial stress distribution function $\Pr(\sigma^*)$ inside the contact. The models are defined in the caption of figure 1.

In Figure 5 we turn our attention back to mean quantities and address the question of how well the various parameterizations predict the (reduced) mean contact stress $\bar{\sigma}_c^*$ as a function of p^*. This time, model 2 gives a slightly better value than model 3, however, only in the asymptotic small-pressure limit. In the cross-over region, model 3 outperforms model 2.

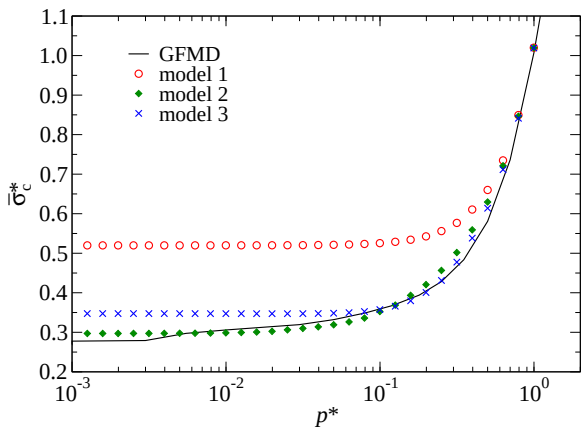

Fig. 5 Reduced, mean contact stress $\bar{\sigma}_c^*$ as a function of the nominal pressure p^*. The models are defined in the caption of figure 1.

It may be interesting to note that Persson found a slight increase of $\bar{\sigma}_c^*$ with decreasing p^* in his submission to the contact challenge, see Figure 11 in reference [29]. We observe a similar trend if the number of

bins used in the generation of the stress histogram is small. Once the discretization of the stress histogram is sufficiently refined, the derivative of $\sigma_c^*(p^*)$ turns out non-negative.

Our final comparison to the contact-mechanics-challenge data pertains to the prediction of the mean gap as a function of pressure. Figure (6) contains results for the high-pressure regime. One can recognize an essentially perfect agreement between Persson theory and the GFMD reference data, in particular that based on model 3 in the limit of large pressures. Persson's own submission is almost indistinguishable from model 2. At small pressure, Persson theory overestimates the mean gap, which is more clearly revealed in the representation chosen for Fig. 12 in reference [29]. We argue that this is because it is implicitly based on the assumption of a thermodynamic limit, for which no strict upper bound of $\bar{u}$ exists.

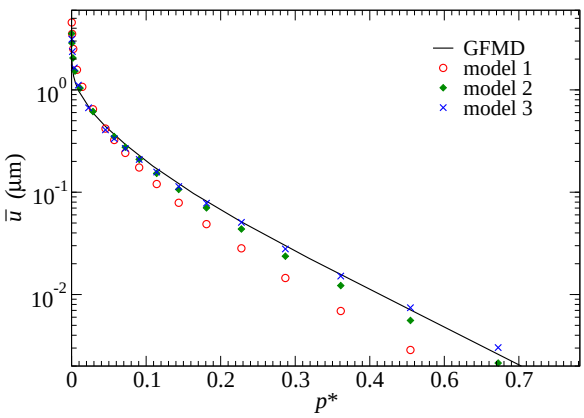

Fig. 6 Mean gap $\tilde{u}$ as a function of p^*. The models are defined in the caption of figure 1.

3.2 Comparison to data of finite-slab geometries

The adhesion used in the contact-mechanics challenge was relatively weak so that it only lead to a 50% increase of the true contact area at small loads compared to the non-adhesive analogue. In addition, the geometry was confined to be that of a semi-infinite elastic solid. To explore how well stress distributions and other properties are predicted by the theory when adhesion becomes more significant or elastic slabs rather thin, we run additional simulations towards this end.

Before presenting results, we contrast two dimensionless measures of adhesion for the two studied systems, namely that of the relatively large-scale contact-mechanics challenge (system I) and the smaller-scale surface (system II) described in section 2.4. The first measure is a local one and is defined as

$$\tilde{\gamma}_{\rm loc} = \frac{\gamma}{E^* R_c \bar{g}^3}. \tag{23}$$

Numerical numbers are $\tilde{\gamma}_{\rm loc}(\mathrm{I}) \approx 1$ and $\tilde{\gamma}_{\rm loc}(\mathrm{II}) \approx 0.1$. The second measure is a global parameter and taken to be the ratio of surface energy and the areal elastic-energy density needed to make full contact, $u_{\rm ela}^{(\rm f)}$, i.e.,

$$\tilde{\gamma}_{\rm glo} = \frac{\gamma}{u_{\rm ela}^{(f)}}. \tag{24}$$

This time, numbers are $\tilde{\gamma}_{\rm glo}(\mathrm{I}) \approx 0.025$ and $\tilde{\gamma}_{\rm glo}(\mathrm{II}) \approx 0.1$. When the thickness of the slab is reduced (with a constant-stress boundary condition at the opposite side of the interface), the global measure decreases, while the local one remains unchanged. To give an example, $\tilde{\gamma}_{\rm glo}(\mathrm{II})$ increases to 0.3 when the thickness t of the elastic manifold is reduced from semi-infinite to $1/4q_r$ and then quickly grows more upon a further reduction of t, while the local measure $\tilde{\gamma}_{\rm loc}$ remains unchanged.

Our simulations reveal that the relative contact area at the reduced pressure of $p^* = 0.01$ is significantly larger for system II than for system I and that the parameterization of Persson theory presented in section 2.3 and tested in section 3.2 underestimates the large adhesion-induced increase of a_r for thick slabs. Rather minor modifications of the parameterization, which are realized in model 4, dramatically reduce that problem, as shown in figure 7. The weight function in model 4 is taken to be $W(a_r) = 0.35 + 0.65(1 - a_r^2)$ and the broadening of Δp is now multiplied with $W^{1/4}(a_r)$ rather than with $W^{1/2}(a_r)$. The fine-tuning of the parameters for the new, highly-adhesive, thin-slab geometry only means redefining parameters by $O(10\%)$, the most dramatic change being $W(a_r \to 0)$ which is equal to 0.35 in model 4 versus 5/9 in model 3.

It is interesting to note that the true contact area in system II at $p^* = 0.005$ would only slightly exceed 1% for the semi-infinite, adhesionless solid and finite-thickness corrections for it would only become relevant for extremely thin slabs. The adhesion-induced increase of contact (in the semi-infinite case) thus is a factor of three, compared to a mere 50% increase of system I, although system II has the larger value of $\tilde{\gamma}_{\rm loc}$. We can therefore no longer claim that $\tilde{\gamma}_{\rm loc}$ is a strong indicator [34] for the increase of true contact. The more meaningful parameter appears to be the global measure for adhesion. In the calculation of the elastic energy, it places more emphasis on long than on short wavelengths for $H > 0.5$ [30]. At this point, we cannot speculate if $\tilde{\gamma}_{\rm glo}$ might also indicate how sticky surfaces are. Recently, Pastweka and Robbins proposed a

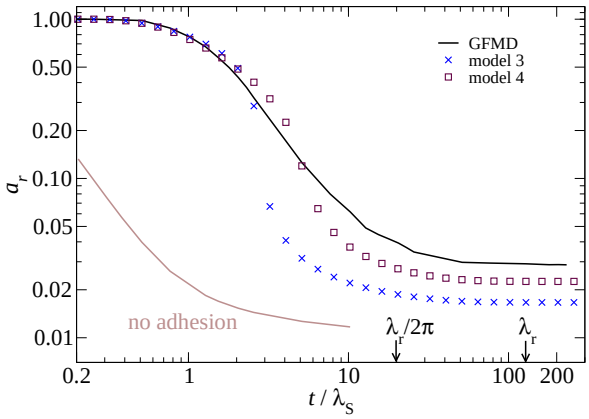

Fig. 7 Relative contact area of system II at a reduced pressure of $p^* = 0.005$ from GFMD simulations and Persson theory with two different parameterizations (models 3 and 4). A reference curve is shown for comparison, in which adhesion in system II is not considered.

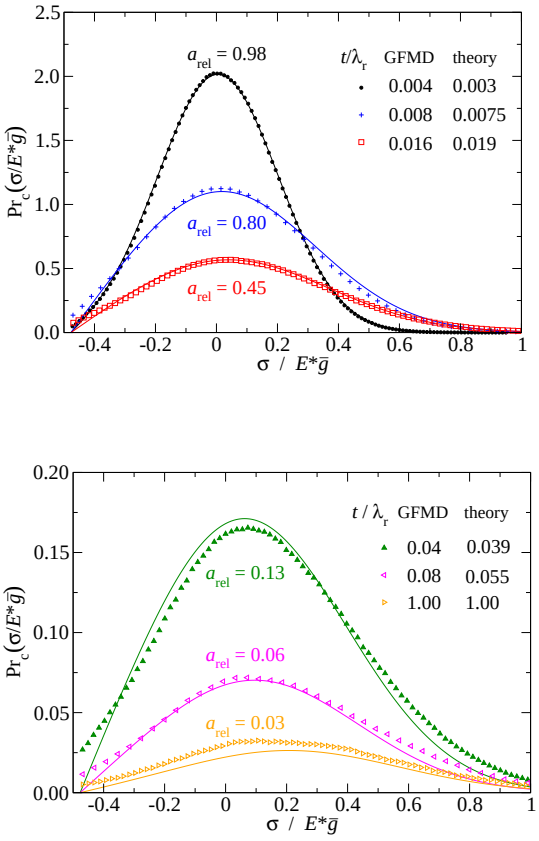

Fig. 8 Interfacial stress distributions for system II at various thicknesses. Symbols show GFMD results, while lines represent the theory, which is based on the parameterization of model 4. The top and bottom graph contain data on thin and thick slabs, respectively. The values stated for the relative contact area a_r area, which is obtained as the integral over $\Pr(\sigma)$, pertain to the GFMD simulation.

local criterion [35], which seemed reliable at least up to medium-scale system sizes.

Since a_r is only a scalar property, we also investigate to what extent the the theory using the parameterization of model 4 reflects the full simulations. To better reveal the trends, we compare $\Pr(\sigma)$ between GFMD and theory at similar contact areas in figure 8.

As is the case for other quantities, Persson theory reproduces the results on stress-distributions from brute-force simulations quite closely if one allows the parameters in the theory to be tweaked by a few percent. Most importantly, the functional forms of $\Pr(\sigma)$ are reproduced quite accurately even if the asymptotic behavior for the largest allowed tensile load may not be perfect. However, it seems as if the presence of adhesion somewhat reduces this issue compared to the results reported in Figure 3.

4 Conclusions

In this paper, we have proposed three modifications of Persson's contact mechanics theory. First, we modified a weight function relating the elastic energy to the surface height spectrum depending on the resolution-dependent relative contact. Second, and more importantly, the weight function now also affects the way in which the pressure distribution broadens with increasing resolution. Finally, we fine-tuned the Griffith criterion used in the theory. These alterations lead to an overall improvement of predictions made with this theory for moderate adhesion and semi-infinite substrates. Most quantities of interest can be predicted within a few percent uncertainty, such as the mean contact stress, or the mean interfacial separation. As such, we support the claim that Persson theory can predict the functional dependence of most functions of interest correctly. For large adhesion (leading to a distinctly increased contact area compared to the adhesionless case), parameters had to be changed again by a few 10% to find a true quantitative agreement between theory and full simulations.

However, we also identified the first case of an incorrect exponent in Persson theory: The stress distribution $\Pr(\sigma)$ increases slightly sub-linearly with σ at small values of σ, while the theory predicts linearity, no matter how the weighting function are fine tuned. We believe that these features arise in real space from the zones near the contact lines. Persson theory implicitly assumes the same stress broadening in the vicinity of contact lines as deep inside the contact and no reentrance of lost contact upon an increase of resolution.

These assumptions have been shown to be approximative [32], however, any numerically feasible theory must make such compromises. It seems, however, that this type of shortcoming is less prominent when adhesion is included into the treatment. This might be beneficial for the modeling of adhesive systems of practical relevance [36,37].

We are aware of previous tests of Persson theory that are not quite as favorable as ours [38]. However, these are based on correlated noise or even deterministic features. In such cases, one might want to apply Persson theory only at scales that are sufficiently small for the smaller-scale roughness features to be described as randomly rough.

The current work covers an unusually broad parameter space. Surface energies and (linear) system size were varied over one decade, load and thickness of the solids over several orders of magnitude. In all tested regimes, the theory performed quite impressively, however, only when fine tuning the value of the three adjustable parameters, which, however, always remained of order unity.

It is certainly somewhat unsatisfactory that some fine-tuning of employed parameters is needed to make truly accurate predictions with Persson theory. The situation can be compared to that of density-functional theory (DFT) in quantum chemistry, where different functionals (and pseudopotentials) also show different performance on different elements. Both theories can be made exact in principle. In DFT, there exists a functional giving the exact ground-state energy (we just do not know the functional) [39], while the basic ideas of Persson theory can be motivated from the leading-order term of a rigorous cumulant expansion [40]. In both cases, however, it seems a non-trivial exercise to find formulations of the theories that are very precise, computationally lean and, at the same time, not in need of some fine readjustments that depend on the system under consideration.

A Stress variance in full contact

Consider single-sinusoidal roughness in a periodically repeated domain of an isotropic, semi-infinite half space:

$$h(\mathbf{r}) = h(\mathbf{q})e^{i\mathbf{q}\cdot\mathbf{r}}. \tag{25}$$

The stress then reads

$$\sigma_{\mathbf{q}}(\mathbf{r}) = i\frac{qE^*}{2}h(\mathbf{q})e^{i\mathbf{q}\cdot\mathbf{r}} \tag{26}$$

so that its variance, averaged over the domain, becomes

$$\Delta\sigma^2_{\mathbf{q}} = \left(\frac{qE^*}{2}\right)|h(\mathbf{q})|^2, \tag{27}$$

If the roughness is spanned by several $\mathbf{q}$ vectors, their stress variances add up due to the orthogonality of $\exp(i\mathbf{q}\cdot\mathbf{r})$ and $\exp(i\mathbf{q}'\cdot\mathbf{r})$ for $\mathbf{q}\neq\mathbf{q}'$. The total stress variance then becomes

$$\Delta\sigma^2_{\mathrm{tot}} = \sum_{\mathbf{q}}\left(\frac{qE^*}{2}\right)^2|h(\mathbf{q})|^2 \tag{28}$$

$$\to \frac{A}{(2\pi)^2}\int d^2q\left(\frac{qE^*}{2}\right)^2|h(\mathbf{q})|^2. \tag{29}$$

In the transition from a discrete to a continuum theory, we have assumed that the $|h(\mathbf{q})|^2$ (more precisely, their expectation values or, alternatively, their running averages) are smooth functions of $\mathbf{q}$. Defining the spectrum to be $C(q) = A|h(\mathbf{q})|^2/(2\pi)^2$, we obtain Persson's expression for the stress variance in full contact [1], namely

$$\Delta\sigma^2_{\mathrm{tot}} = \int d^2q\left(\frac{qE^*}{2}\right)^2 C(\mathbf{q}), \tag{30}$$

which is proportional to the mean-square surface gradient [6]. Calculations for sheets of finite thickness t can be done in a similar fashion by multiplying a weighting factor $f(qt)$ to E^*.

B Derivation of the kernel function

The diffusion equation

$$D\partial_x^2 T(x,t) = \partial_t T(x,t), \tag{31}$$

subjected to the absorbing boundary condition $T(x = x_{\mathrm{a}}, t) = 0$ can be solved as a Sturm-Liouville problem with the sine Fourier transform

$$T(x,t) = \sqrt{\frac{2}{\pi}}\int_0^\infty dq\,\tilde{T}(q,t)\sin\{q(x-x_{\mathrm{a}})\}. \tag{32}$$

The Fourier coefficients thus obey

$$-Dq^2\tilde{T}(q,t) = \partial_t\tilde{T}(q,t) \tag{33}$$

so that

$$\tilde{T}(q,t) = \tilde{T}(q,0)e^{-q^2Dt}. \tag{34}$$

The solution for a general initial condition then reads

$$T(x,t) = \sqrt{\frac{2}{\pi}}\int_0^\infty dq\,\tilde{T}(q,0)\sin\{q(x-x_{\mathrm{a}})\}e^{-q^2Dt}. \tag{35}$$

The left-hand side of this equation turns into a kernel function if the initial condition for $T(x,t=0)$ is a delta-function, $\delta(x-x_0)$, in which case

$$\begin{aligned} K(x,x_0,t) &= \frac{2}{\pi}\int_0^\infty dq\,\sin\{q(x_0-x_{\mathrm{a}})\}\sin\{q(x-x_{\mathrm{a}})\}e^{-q^2Dt} \\ &= \frac{e^{-(x-x_0)^2/2\sigma^2} - e^{-(x+x_0+2x_{\mathrm{a}})^2/2\sigma^2}}{\sqrt{2\pi\sigma^2}} \end{aligned} \tag{36}$$

with $\sigma^2 = 2Dt$. Note that similar equations hold if the initial time is different from zero.

The second term on the right-hand side of Eq. (36) is what we call the mirror Gaussian in the main text. To make full connection to the main text, please substitute, amongst other expressions, $\sigma^2 \to \Delta p^2$, $x_{\mathrm{a}} \to -\sigma_{\mathrm{a}}^+$, and $T(x,t) \to \Pr(\sigma, q)$.

Acknowledgments MHM thanks Bo Persson for helpful discussions, Nikolay Prodanov and Wolf Dapp for technical support in the initial phases of the project, the German research foundation (DFG) for financial support through grant Mu 1694/5-1, and the Jülich Supercomputing Centre for computing time on JUQUEEN.

References

1. B. N. J. Persson. Theory of rubber friction and contact mechanics. *The Journal of Chemical Physics*, 115(8):3840, 2001.
2. B.N.J. Persson. Contact mechanics for randomly rough surfaces. *Surface Science Reports*, 61(4):201–227, jun 2006.
3. J. F. Archard. Elastic deformation and the laws of friction. *Proceedings of the Royal Society A: Mathematical, Physical and Engineering Sciences*, 243(1233):190–205, dec 1957.
4. J. A. Greenwood and J. B. P. Williamson. Contact of nominally flat surfaces. *Proceedings of the Royal Society A: Mathematical, Physical and Engineering Sciences*, 295(1442):300–319, dec 1966.
5. A.W. Bush, R.D. Gibson, and T.R. Thomas. The elastic contact of a rough surface. *Wear*, 35(1):87–111, nov 1975.
6. S. Hyun, L. Pei, J.-F. Molinari, and M. O. Robbins. Finite-element analysis of contact between elastic self-affine surfaces. *Physical Review E*, 70(2):026117, aug 2004.
7. C Campañá and M. H Müser. Contact mechanics of real vs. randomly rough surfaces: A Green's function molecular dynamics study. *Europhysics Letters (EPL)*, 77(3):38005, jan 2007.
8. G. Carbone and F. Bottiglione. Asperity contact theories: Do they predict linearity between contact area and load? *Journal of the Mechanics and Physics of Solids*, 56(8):2555–2572, aug 2008.
9. Marco Paggi and Michele Ciavarella. The coefficient of proportionality κ between real contact area and load, with new asperity models. *Wear*, 268(7-8):1020–1029, mar 2010.
10. C. Putignano, L. Afferrante, G. Carbone, and G. Demelio. The influence of the statistical properties of self-affine surfaces in elastic contacts: A numerical investigation. *Journal of the Mechanics and Physics of Solids*, 60(5):973–982, may 2012.
11. Nikolay Prodanov, Wolf B. Dapp, and Martin H. Müser. On the contact area and mean gap of rough, elastic contacts: Dimensional analysis, numerical corrections, and reference data. *Tribology Letters*, 53(2):433–448, dec 2013.
12. Roman Pohrt, Valentin L. Popov, and Alexander E. Filippov. Normal contact stiffness of elastic solids with fractal rough surfaces for one- and three-dimensional systems. *Physical Review E*, 86(2):026710, aug 2012.
13. Lars Pastewka, Nikolay Prodanov, Boris Lorenz, Martin H. Müser, Mark O. Robbins, and Bo N. J. Persson. Finite-size scaling in the interfacial stiffness of rough elastic contacts. *Physical Review E*, 87(6):062809, jun 2013.
14. C. Yang and B. N. J. Persson. Contact mechanics: contact area and interfacial separation from small contact to full contact. *Journal of Physics: Condensed Matter*, 20(21):215214, 2008.
15. Lars Pastewka and Mark O. Robbins. Contact area of rough spheres: Large scale simulations and simple scaling laws. *Applied Physics Letters*, 108(22):221601, may 2016.
16. Martin H. Müser. On the contact area of nominally flat hertzian contacts. *Tribology Letters*, 64(1):14, sep 2016.
17. A. Almqvist, C. Campañá, N. Prodanov, and B.N.J. Persson. Interfacial separation between elastic solids with randomly rough surfaces: Comparison between theory and numerical techniques. *Journal of the Mechanics and Physics of Solids*, 59(11):2355–2369, nov 2011.
18. C Campañá, B N J Persson, and M H Müser. Transverse and normal interfacial stiffness of solids with randomly rough surfaces. *Journal of Physics: Condensed Matter*, 23(8):085001, feb 2011.
19. Wolf B. Dapp, Andreas Lücke, Bo N. J. Persson, and Martin H. Müser. Self-affine elastic contacts: Percolation and leakage. *Phys. Rev. Lett.*, 108(24):244301, jun 2012.
20. Wolf B. Dapp and Martin H. Müser. Fluid leakage near the percolation threshold. *Scientific Reports*, 6(1):19513, feb 2016.
21. B N J Persson. On the elastic energy and stress correlation in the contact between elastic solids with randomly rough surfaces. *Journal of Physics: Condensed Matter*, 20(31):312001, jun 2008.
22. Carlos Campañá, Martin H Müser, and Mark O Robbins. Elastic contact between self-affine surfaces: comparison of numerical stress and contact correlation functions with analytic predictions. *Journal of Physics: Condensed Matter*, 20(35):354013, aug 2008.
23. G. Carbone, L. Mangialardi, and B. N. J. Persson. Adhesion between a thin elastic plate and a hard randomly rough substrate. *Physical Review B*, 70(12):125407, sep 2004.
24. C. Yang, B. N. J. Persson, J. Israelachvili, and K. Rosenberg. Contact mechanics with adhesion: Interfacial separation and contact area. *EPL (Europhysics Letters)*, 84(4):46004, nov 2008.
25. B. N. J. Persson and M. Scaraggi. Theory of adhesion: Role of surface roughness. *The Journal of Chemical Physics*, 141(12):124701, sep 2014.
26. G. Carbone, B. Lorenz, B. N. J. Persson, and A. Wohlers. Contact mechanics and rubber friction for randomly rough surfaces with anisotropic statistical properties. *The European Physical Journal E*, 29(3):275–284, jul 2009.
27. B. N. J. Persson. Elastoplastic contact between randomly rough surfaces. *Physical Review Letters*, 87(11):116101, aug 2001.
28. G. Carbone, M. Scaraggi, and U. Tartaglino. Adhesive contact of rough surfaces: Comparison between numerical calculations and analytical theories. *The European Physical Journal E*, 30(1):65–74, sep 2009.
29. M. H. Müser, W. B. Dapp, and other challenge participants. To be filled in by editor.
30. B.N.J. Persson. Adhesion between an elastic body and a randomly rough hard surface. *The European Physical Journal E*, 8(4):385–401, jul 2002.
31. W. Manners and J.A. Greenwood. "some observations on persson's diffusion theory of elastic contact". *Wear*, 261(5-6):600–610, sep 2006.
32. Wolf B Dapp, Nikolay Prodanov, and Martin H Müser. Systematic analysis of persson's contact mechanics theory of randomly rough elastic surfaces. *Journal of Physics: Condensed Matter*, 26(35):355002, jul 2014.
33. Carlos Campañá and Martin H. Müser. Practical Green's function approach to the simulation of elastic semi-infinite solids. *Phys. Rev. B*, 74(7):075420, aug 2006.
34. Martin H. Müser. A dimensionless measure for adhesion and effects of the range of adhesion in contacts of nominally flat surfaces. *Tribology International*, 100:41–47, aug 2016.
35. Lars Pastewka and Mark O. Robbins. Contact between rough surfaces and a criterion for macroscopic adhesion. *Proceedings of the National Academy of Sciences*, 111(9):3298–3303, feb 2014.
36. Sarah C. L. Fischer, Eduard Arzt, and René Hensel. Composite pillars with a tunable interface for adhesion to rough substrates. *ACS Applied Materials & Interfaces*, 9(1):1036–1044, jan 2017.
37. Ram Gopal Balijepalli, Sarah C.L. Fischer, René Hensel, Robert M. McMeeking, and Eduard Arzt. Numerical study of adhesion enhancement by composite fibrils with

soft tip layers. *Journal of the Mechanics and Physics of Solids*, 99:357–378, feb 2017.
38. Robert L. Jackson and Itzhak Green. On the modeling of elastic contact between rough surfaces. *Tribology Transactions*, 54(2):300–314, jan 2011.
39. P. Hohenberg and W. Kohn. Inhomogeneous electron gas. *Physical Review*, 136(3B):B864–B871, nov 1964.
40. Martin H. Müser. Rigorous field-theoretical approach to the contact mechanics of rough elastic solids. *Physical Review Letters*, 100(5), feb 2008.